A&A 382, 1052–1060 (2002)
DOI: 10.1051/0004-6361:20011678

Astronomy & Astrophysics

ASCA observation of X-ray emission from the Galactic ridge

Y. Tanaka⋆

[1] Max-Planck-Institut für Extraterrestrische Physik, 85748 Garching, Germany
[2] Institute of Space and Astronautical Science, Sagamihara, Kanagawa 229, Japan

Received 4 October 2001 / Accepted 22 November 2001

Abstract. The recent *Chandra* result confirmed the diffuse origin for the most part of the extended X-ray emission from the Galactic ridge. The ASCA spectrum of the emission shows a hard continuum ($kT \sim 10$ keV if thermal) and the emission lines from highly-ionized ions of various elements up to iron. The thermal origin hypothesis contains fundamental problems concerning heating and confinement of the plasmas, and the energy source. This paper presents the results of renewed analysis of the ASCA SIS spectra of the ridge emission at three places, $l \sim 28.5°, 10°$ and near the Galactic Center. All the observed spectra are found to be essentially identical in shape, indicating the same emission mechanism regardless of the brightness (or the volume emissivity). Thermal emission models, either non-equilibrium or equilibrium ionization, cannot self-consistently explain the observed H-like to He-like K-line intensity ratios of Si, S and Fe. In addition, the He-like and H-like Fe K-lines are significantly broadened, corresponding to a velocity dispersion of a few thousand km s^{-1}. This is much higher than the thermal or bulk motion velocity for plasmas of $kT \sim 10$ keV, and provides strong evidence against the thermal origin of the lines. An alternative possibility of line emission by charge exchange interaction of low-energy cosmic-ray heavy ions has been proposed, which gives natural explanation of the observed line broadening. The low-energy cosmic-ray origin is also consistent with the presence of a non-thermal component in the ridge emission, most probably due to low-energy cosmic-ray electrons. Heavy ions must be accelerated simultaneously with electrons.

Key words. Galaxy: disk – X-rays: diffuse background – X-rays: ISM

1. Introduction

The unresolved X-ray emission along the Galactic ridge has long been known (Worrall et al. 1982). This Galactic ridge X-ray emission (GRXE) extends over the Galactic longitude range between $\sim\pm40°$, coming from a disk-like region of a several-kpc radius from the Galactic center and a scale height of ∼100 pc (e.g. Yamauchi & Koyama 1993). The brightness distribution also shows a prominent peak in the region within a degree around the Galactic center (Yamauchi & Koyama 1993; Koyama et al. 1996). The total luminosity of the GRXE in the range 2–10 keV is $\sim 2 \times 10^{38}$ erg s^{-1}. Despite many years of studies, the origin of the GRXE still remains unsettled.

The most fundamental question is whether the GRXE is of discrete origin or genuinely diffuse. Previous studies found it difficult to explain in terms of a population of any known class of sources (e.g. Kaneda 1997; Tanaka et al. 1999). A decisive result has recently been obtained from a *Chandra* observation of the Galactic plane in the Scutum region ($l = 28.4°$) by Ebisawa et al. (2001). The obtained log N–log S relation down to a flux limit of $\sim 3 \times 10^{-15}$ erg cm^{-2} s^{-1}(2–10 keV) is consistent with most of the detected sources being extragalactic, hence the Galactic source contribution is negligibly small. Thus, they conclude that most of the GRXE is diffuse emission.

Extensive observations of the GRXE with ASCA show that its spectrum varies little with Galactic longitude (Kaneda 1997). The observed spectrum revealed intense emission lines from highly ionized ions of various elements, which motivated interpretation of the GRXE as the thermal emission from high-temperature plasmas. Another important property of the GRXE spectrum is the presence of a hard power-law tail that was first pointed out by Yamasaki et al. (1994) and later established by Valinia et al. (2000a) to at least 300 keV. Obviously, this hard tail is of non-thermal origin.

Kaneda (1997) and Kaneda et al. (1997) explained the GRXE spectrum observed with ASCA (mainly those obtained with the ASCA GIS) below 10 keV with two (a soft and a hard) thermal plasma components of significant non-equilibrium ionization (*nei*), with the estimated temperatures of the two components at $kT \sim 0.8$ keV and ∼7 keV, respectively. They state that the soft component can be accounted for by supernova remnants. Whereas, the origin of the hard component remains uncertain.

If the GRXE is due to extended interstellar plasmas, several problems arise: (1) How to heat up the plasmas to $kT \sim 10$ keV, much hotter than young supernova

⋆ e-mail: ytanaka@mpe.mpg.de

remnants? (2) The energy density of the plasma ($\sim$100 eV cm^{-3}) is nearly two orders of magnitude higher than those of interstellar matter, cosmic rays and magnetic fields, i.e. far from equipartition and far from pressure balance with other interstellar constituents. (3) These plasmas cannot be confined with the general interstellar magnetic fields of several μGauss, hence will escape out of the plane. The energy loss rate of the mass outflow is huge, $\sim 10^{43}$ erg s^{-1}, corresponding to a rate of 1 supernova/yr. What is the energy source?

Makishima (1997) considered a possibility that a fraction of cooler plasma is heated through magnetic compression and reconnection induced by the Galactic rotation. Tanuma et al. (1999) studied magnetic reconnection triggered by a supernova, and showed that plasma could be heated to $kT \sim 10$ keV and confined by a flux tube with $B_{\rm local} \sim 30$ μGauss. Such a process will produce a localized bright X-ray structure. On the other hand, the observed surface brightness distribution is rather smooth, and such distinct structures with $kT \sim 10$ keV have not been found.

In order to resolve the issue of the origin of the GRXE, a further attempt is made for finding clues from the observed GRXE spectrum obtained with the ASCA SIS instrument. The SIS has superior energy resolution (a factor of $\sim$4 better than the GIS) and can resolve the He-like and the H-like lines as well as the lower-ionization lines from each element. (See Tanaka et al. 1994 and Burke et al. 1995 for more details.)

2. ASCA SIS Spectra

Long-exposure data are available for three places on the Galactic plane ($|b| \leq 0.5^\circ$); a Scutum (Sct) region ($l \cong 28.5^\circ$), a Sagittarius (Sgr) region ($l \cong 10^\circ$), and a region within 1° around the Galactic center (GC). The SIS suffered long-term degradation of energy resolution in orbit due to radiation damage. However, these observations were carried out late 1993 when the energy resolution was still near its best. The ASCA SIS results on the GC region were reported by Koyama et al. (1996) and Tanaka et al. (2000), and on the Sct region by Kaneda et al. (1997). In this work, the archival SIS data for the Sgr and Sct regions are reanalyzed for a detailed study of the spectrum, in particular the iron line structure, with an accurate energy scale calibration. The observation log is given in Table 1.

A bright transient source was detected (designated AX J1845.0-0433) in the observation of the Sct region No. 3, hence the data of the whole CCD chip containing the source were excluded from the analysis. A few other faint sources are found in the Sct field (Yamauchi et al. 1996). They are not excluded, since their contributions are negligibly small. The data of the Sgr region were from the observations in order to determine the position of the soft gamma-ray repeater SGR 1806-20 during its burst activity. A relatively weak X-ray source was detected coincident with the burst location (Murakami et al. 1994). The data within 3′-radius of the source were excluded. No other

Table 1. Observation log for the Sgr and Sct regions.

Obs. No.	l	b	Date	SIS Exposure (ks)
Sgr No. 1	10.19°	−0.03°	Oct 09 '93	14.0
Sgr No. 2	9.26°	−0.53°	Oct 10 '93	13.3
Sgr No. 3	9.57°	−0.37°	Oct 10 '93	19.2
Sgr No. 4	9.89°	−0.21°	Oct 11 '93	28.6
Sgr No. 5	"	"	Oct 20 '93	37.6
Sct No. 1	28.25°	+0.49°	Oct 18 '93	22.7
Sct No. 2	28.25°	+0.02°	Oct 19 '93	20.8
Sct No. 3	28.25°	−0.44°	Oct 19 '93	21.9
Sct No. 4	28.72°	−0.44°	Oct 21 '93	22.3
Sct No. 5	28.72°	+0.02°	Oct 22 '93	21.6
Sct No. 6	28.72°	+0.49°	Oct 24 '93	19.7

significant point sources are in the field of view. After the standard data screening process, all the events (eight CCD chips of SIS0 and SIS1) are summed for each region. The total lengths of useful exposure are $\sim$120 ks and $\sim$80 ks for the Sct region and the Sgr region, respectively.

The background consists of the internal background (IB) and the cosmic X-ray background (CXRB). The former dominates above $\sim$6 keV and has prominent particle-induced fluorescence lines such as Fe-Kα (6.40 keV), Fe-Kβ (7.06 keV), Ni-Kα (7.48 keV) (see Gendreau et al. 1995, and also Fig. 3). The IB changes its level depending on the particle environment, hence accurate IB subtraction is important, in particular for the study of the iron lines. Here, the IB spectrum is derived in the following way, instead of using the night-earth spectrum of low statistical quality available. It is an inverse process of Gendreau et al. (1995) who determined the CXRB spectrum from the "blank (source-free) sky" spectrum of low absorption, by modeling the IB spectrum. The "statistical" data of the IB is obtained by subtracting the best-fit CXRB model spectrum from the "blank sky" spectrum. The thus-obtained IB spectrum maintains the complex features above $\sim$6 keV untouched. The IB level to be subtracted is determined so as the Ni-Kα (7.48 keV) line intensity to be equal to that observed. This line is distinctly visible in all the observed spectra and is well separated from the Fe lines, hence also useful for precise calibrations of the energy scale and resolution. In the following analysis, the CXRB is treated as a fixed model component with proper interstellar absorption.

The observed spectra for the two regions after IB subtraction are shown in Figs. 1a and b. The CXRB contribution is also plotted in each figure. The HI column density is $\sim 2 \times 10^{22}$ cm^{-2} (Dickey & Lockman 1990) and that of H_2 is roughly $(1-2) \times 10^{22}$ cm^{-2} (Dame et al. 2001) for both regions. A total hydrogen column density $N_{\rm H}$ of 4×10^{22} cm^{-2} is assumed for the absorption of the CXRB. The results of the following analysis is insensitive to the assumed $N_{\rm H}$-value within $\pm 2 \times 10^{22}$ cm^{-2}. These spectra exhibit prominent emission lines from highly-ionized

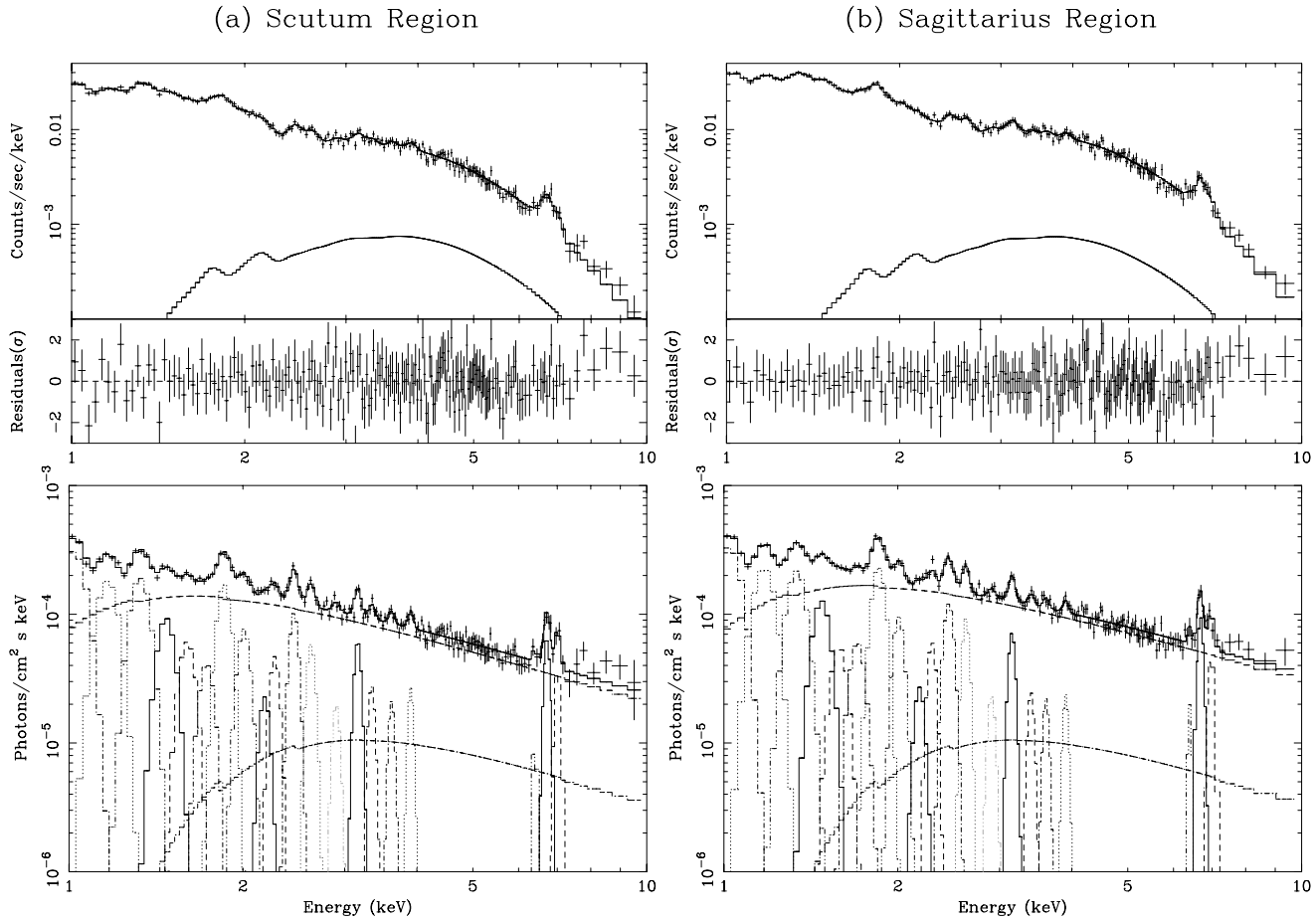

Fig. 1. The ASCA SIS spectra of **a)** the Sct region and **b)** the Sagittarius region. The upper panels show the observed spectra together with the best-fit models and the assumed CXRB contributions. The lower panels are the unfolded photon spectra for the instrument response. The continuum, the Gaussian lines and the CXRB are also plotted.

ions on top of a hard continuum. Previously Kaneda et al. (1997) identified these lines for the Sct region (Fig. 1a) with the He-like and/or H-like Kα lines of Ne, Mg, Si, S, Ar and Fe, and determined the equivalent widths.

For characterizing the observed spectra, we employ a simple model consisting of a continuum and multiple lines of Gaussian form. A single power law modified with absorption by a column $N_{\rm H}*$ (see below) well represents the continuum. For emission lines, all major lines, not only the He-like and H-like Kα lines but also the He-like Kβ lines, and some Fe L-lines, that are previously identified in the spectrum of the GC region (Tanaka et al. 2000) are included. This model gives good fits to the observed spectra with χ^2/ν of 174/184 for the Sgr region and 207/210 for the Sct region, as shown in Figs. 1a and b.

In the course of the fitting, unambiguous determination of the line intensities is found to be difficult in the energy range below 2 keV where many lines, complex Fe L-lines in addition to K-lines of Ne Mg, may exist. Because of the limited SIS resolution, these line profiles overlap with each other and hide the base line continuum (coupled with $N_{\rm H}^*$, see below), causing fair uncertainties. On the other hand, the ratio of the intensities of the He-like and H-like line is relatively insensitive to this problem at least for Si and S. In addition, the Fe K-line appears as a single broad line, which is separately analyzed in detail. These intensity ratios together with the best-fit power-law parameter values are listed in Table 2 (the line ratios of Fe are those obtained by a separate analysis, see Table 3). It is to be noted that the assumption of a single foreground absorption is physically unrealistic, because the emission regions may not be localized but most probably intermingled with interstellar absorber along the line of sight. However, it can be shown that the integrated spectrum of distributed emission and absorption is approximately expressed by the simple form employed, if $\sigma(E)N_{\rm H} < 1$, where $\sigma(E)$ is the interstellar absorption cross section per hydrogen atom and $N_{\rm H}$ the total hydrogen column on the line of sight (Kaneda 1997). The "effective" absorption column denoted by $N_{\rm H}^*$ is much smaller than $N_{\rm H}$.

Except for a brightness difference, the Sgr region being a factor of $\sim$1.3 brighter than the Sct region, the spectra of the two regions are almost identical. Furthermore, their characteristic spectral features appear strikingly similar to those observed in the GC region (Koyama et al. 1996; Tanaka et al. 2000). The surface brightness in the GC region peaks in the Sgr A shell, and falls steeply within a degree and connects to the outer GRXE. The spectral shape

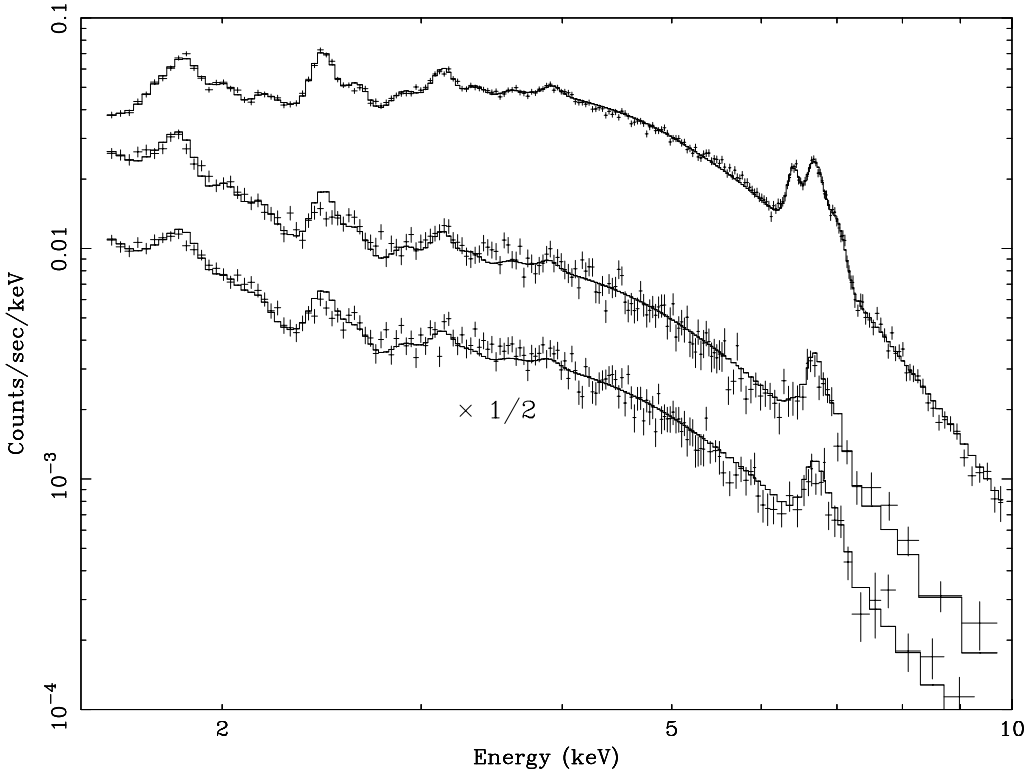

Fig. 2. Comparison of the observed spectra in the three regions; the GC region (top), the Sgr region (middle) and the Sct region (bottom: shifted down by a factor of 2). The overlaid model curves are the best-fit to the GC region spectrum, which are all the same except for the absorption, normalization, and the 6.4-keV line intensity.

Table 2. Power-law indices, $N_{\rm H}^{*}$-values, and H-like to He-like Kα line intensity ratios of Si, S and Fe for three regions.

Region	power-law index	$N_{\rm H}^{*}$	I(H-like)/I(He-like)		
		10^{22} cm^{-2}	Si	S	Fe †
Sct	1.32 ± 0.20	0.7 ± 0.6	0.39 ± 0.10	0.55 ± 0.21	0.48 ± 0.30
Sgr	1.28 ± 0.14	0.9 ± 0.4	0.28 ± 0.10	0.59 ± 0.22	0.44 ± 0.25
GC	1.20 ± 0.04	3.7 ± 0.2	0.35 ± 0.03	0.33 ± 0.04	0.51 ± 0.06

† The values for the Fe-lines are obtained from a separate analysis, see Table 3.

is found to remain constant over the entire $\sim 1^\circ \times 1^\circ$ area excluding the Sgr A shell (Koyama et al. 1996; Tanaka et al. 2000). The average spectrum outside the Sgr A shell is shown in Fig. 2. While the average brightness in the GC region is an order of magnitude higher than those in the Sct and Sgr regions, the observed spectral shapes in these three regions are remarkably close to each other when corrected for absorption, as shown in Fig. 2. For reference, the best-fit model determined for the GC region is overlaid on the spectra of the Sgr and Sct regions after adjusting only the amount of absorption, normalization and the 6.4-keV line intensity by fitting. Here, the energy range is limited above 1.6 keV (excluding the Mg K-lines and below), since the absorption in lower energies becomes too large to justify a simple foreground absorber approximation (see above) and also the foreground GRXE contribution becomes significant. In this fitting, the best-fit $N_{\rm H}^{*}$ values are 1.1×10^{22} cm^{-2} for the Sct region and 1.3×10^{22} cm^{-2} for the Sgr region, which are a little larger than but consistent with those given in Table 2.

One cannot yet claim that the fit of the model spectrum of the GC region to the spectra of the other two regions is perfect. An apparent mismatch is noticed for the S K-lines. However, as listed in Table 1, the H-like to He-like line intensity ratios are not inconsistent to be the same within 90% confidence errors. Thus, except for the 6.4-keV Fe line (to be discussed later), one can conclude that all the spectra are essentially identical in shape.

The iron K-lines carry particular importance for the interpretation of the spectrum. Accurate background subtraction is essential for obtaining the iron line structure, because as mentioned earlier the IB spectrum contains not only the neutral Fe Kα line (6.40 keV) but also Kβ line (7.06 keV), the latter being close to the H-like Fe Kα line (6.97 keV). The strong Ni Kα-line at 7.48 keV in the IB provides the precise background level as well as the energy-scale calibration. In addition, the observed width of the 7.48-keV Ni line that is intrinsically narrow allows determination of energy resolution. It is found that the observed 7.48-keV lines for the Sct and Sgr regions are a

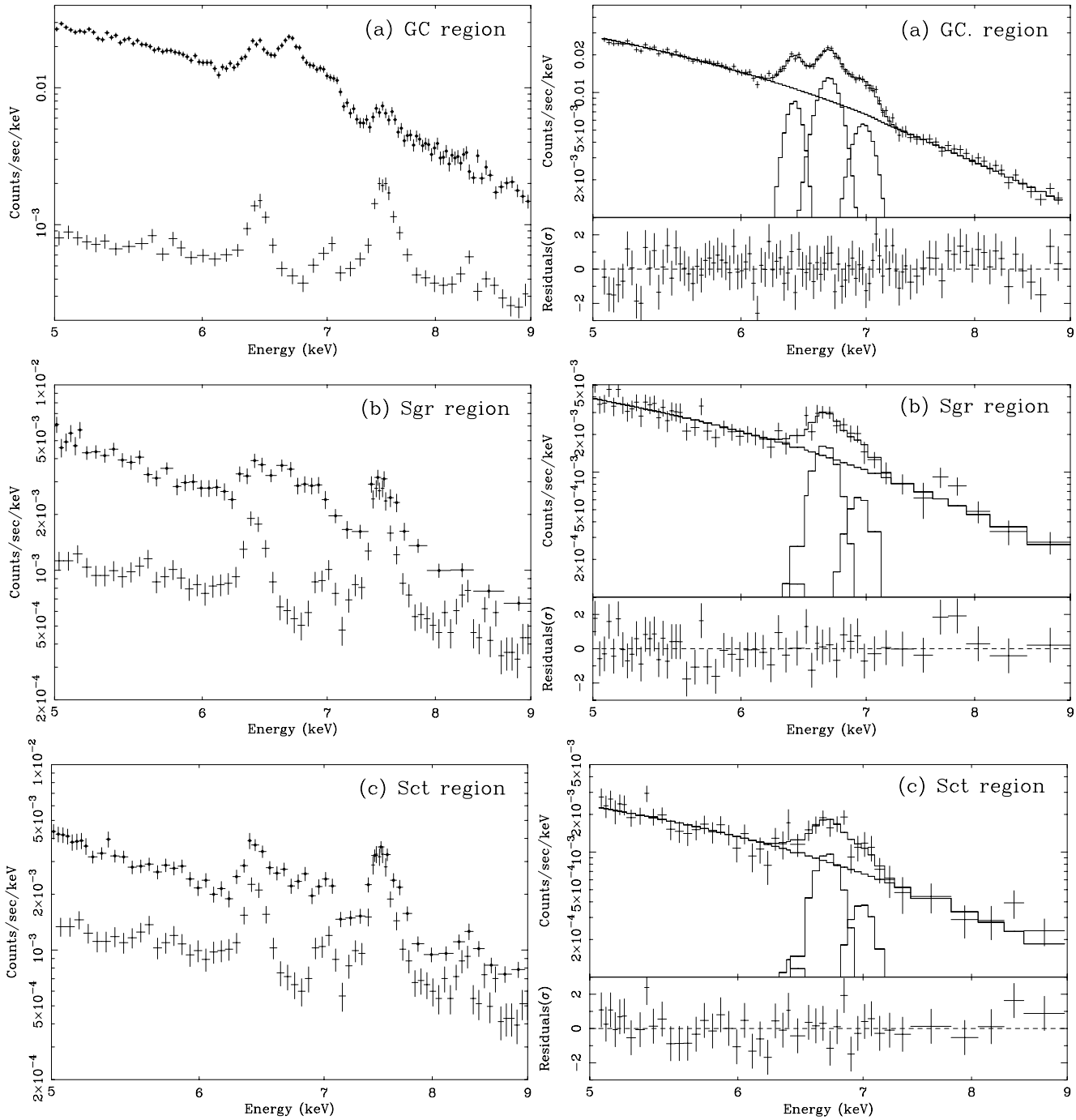

Fig. 3. The observed spectra of the Fe K-lines for **a)** the GC region (excluding the Sgr A shell), **b)** the Sgr region and **c)** the Sct region. The left panels show the observed spectra (filled circle) before background subtraction and the background spectra. The right panels are the spectra after background subtraction and the results of the fit with three lines; the 6.4-keV line, the He-like line (triplet) and the H-like line. The figures for the Sgr and Sct regions are for fixed widths of both the He-like and H-like lines at $\sigma = 70$ eV, equal to that for the GC region (see text).

little broader than in the GC region. This is probably due to less stringent data screening and/or gain correction of the individual chips. The response matrix file (rmf) that describes the energy resolution is modified for each field, in such a way that the observed profile of the Ni line is reproduced with a Gaussian width $\sigma = 0$. Figure 3 shows the observed spectra and the background, and the iron line structures after background subtraction, for the three regions.

Figure 3a shows the observed iron-line structure in the GC region (Tanaka et al. 2000). The 6.4-keV line is intense with an equivalent width of ∼110 eV. This is a narrow line. On the other hand, the He-like (6.70 keV) and H-like (6.97 keV) Kα lines are significantly broader with a Gaussian width $\sigma \approx 70$ eV. The fact that the He-like line is a triplet is taken into account in the analysis (see Tanaka et al. 2000). For the Sgr and Sct regions (Figs. 3b and 3c), an obvious feature is that the 6.4-keV line is much

weaker than in the GC region. In addition, the He-like and H-like lines are not separately visible. If the whole profile is fitted with a single line, it yields the peak energy at approximately 6.76 keV and a Gaussian width $\sigma \sim 170$ eV. However, the extremely large line width and the asymmetric profile obviously indicate that it is a blend of the He-like and H-like lines. For the fitting, the energy of the He-like line is determined as a free parameter, while the ratio of the two line energies is fixed to that of the true value, i.e. 6.97/6.70. In addition, the widths σ of the two lines are assumed to be equal. The 6.4-keV line is also included in the model, and is assumed to be narrow.

Table 3. Observed Fe line energy, equivalent widths, and H-like to He-like line intensity ratio in three regions. The errors are 90% confidence limits.

Region	Line keV	Observed keV	Equiv. width eV	I(H-like)/ I(He-like)
GC	6.40	6.39 ± 0.01	110 ± 10	
	6.70	6.69 ± 0.01	270 ± 20	
	6.97	1.04×above	150 ± 15	0.51 ± 0.06
Sgr	6.40	fixed at 6.40	<50	
	6.70	6.68 ± 0.05	290 ± 60	
	6.97	1.04×above	115 ± 60	0.44 ± 0.25
Sct	6.40	fixed at 6.40	<70	
	6.70	6.69 ± 0.06	280 ± 70	
	6.97	1.04×above	120 ± 70	0.48 ± 0.30
Sct	6.40	fixed at 6.40	<60	
+	6.70	6.69 ± 0.05	330 ± 50	
Sgr	6.97	1.04×above	130 ± 50	0.43 ± 0.18

The results of the fit are listed in Table 3. The observed energy values of the 6.7-keV line are given after applying correction for a slight energy-scale offset, based on the observed energy of the 7.48-keV Ni line. They are in excellent agreement with the true value. Because of the poor statistics for the Sgr and Sct regions, the acceptable range of the line width is fairly wide. The 90% confidence range of σ is obtained to be 40–180 eV for the Sgr region and 30–160 eV for the Sct region. If the data for these two regions are added together, the range is refined to 60–120 eV. This result is fully consistent to be equal to that for the GC region, and excludes narrow lines. Within the acceptable range of σ, the line intensity is somewhat coupled with σ in the fitting process, i.e. the larger the line width, the weaker becomes the H-like line intensity. The equivalent widths of the He-like and H-like lines, and the intensity ratio in Table 3 are the values obtained when the intrinsic line widths σ are fixed at 70 eV determined for the GC region (see Tanaka et al. 2000), allowing for direct comparison. Whereas, the errors are determined dealing σ free. As a result, the line intensity ratios are found to be the same for all three regions, approximately 2:1, within the statistical uncertainties. For the 6.4-keV line, the 90% confidence upper limits of equivalent width are 50 eV and 70 eV for the Sgr and Sct regions, respectively.

3. Discussion

The observed spectra in the Sgr and Sct regions are unique in the following respects: (1) The continuum is very hard. If it is thermal Bremsstrahlung, the temperature is $kT \sim 10$ keV or more, much higher than any of the young SNR. (2) Intense lines of not only Fe but also all abundant lower-Z elements are present. For the thermal emission from such a high temperature plasma in ionization equilibrium, no other lines than those from Fe are significant. Therefore, the plasmas must either be in the state of non-equilibrium ionization (*nei*) or comprise multi-temperature components. These properties are quite unusual among the spectra of known X-ray sources.

Kaneda et al. (1997) reconstructed the GIS spectrum with a two-component *nei* thermal plasma model, consisting of a soft ($kT \sim 0.8$ keV) component and a hard ($kT \sim 7$ keV) component. However, it is found that such a two-component *nei* model does not give an acceptable fit to the observed SIS spectra. This is mainly because the observed H-like to He-like Fe K-line intensity ratio is close to the value in collisional ionization equilibrium (see below). Kaneda et al. (1997) previously reported that the Fe K-line complex showed the center energy at ∼6.61 keV in the Sct region, and attributed it to a blend of the lines from lower ionization states expected from non-equilibrium ionization. However, their center energy is significantly lower than that obtained from the present analysis. The reason for this difference is suspected to be a slight energy-scale offset in their data. In the present analysis, the lines from intermediate ionization states are not required.

As shown in Sect. 2, the observed spectra in all the three regions are found to be essentially identical in shape except for the 6.4-keV Fe line. Considering the unique properties of the spectra, such a close similarity cannot be accidental, and must imply that they are all due to one and the same emission mechanism, and that the diffuse emission near the G.C. is part of the GRXE. Kaneda (1997) found that the spectral shape varies little over a wide range of the Galactic latitude. The present result suggests that the entire GRXE has the same spectral shape.

An immediate consequence of the near identity of the spectral shape is that the *nei* plasma is very unlikely. The intensity ratio of the He-like to H-like lines is sensitive to the quantity $n_e t$ in an *nei* plasma for $n_e t \ll 10^{12}$ s cm^{-3} (as is the case of Kaneda et al. 1997), where n_e and t are the electron density and the age of the plasma, respectively. Hence, similar intensity ratio implies a similar $n_e t$-value. On the other hand, the n_e-value of the GC region (∼0.3 cm^{-3}, Koyama et al. 1996) is two orders of magnitude larger than in the Sct region ($\sim 3 \times 10^{-3}$ cm^{-3}, Kaneda et al. 1997) and the Sgr region (similar to the Sct region because of similar surface brightness). There is no reason why the $n_e t$-values are all similar. For further evidence against *nei*, the observed He-like to H-like Fe line

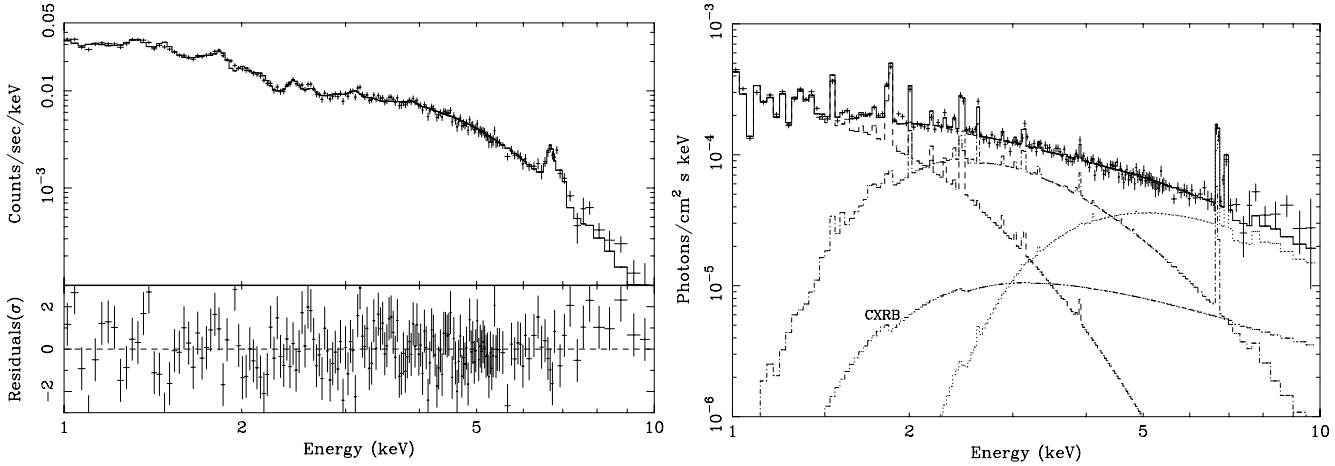

Fig. 4. An example of a model with multi-temperature components. The left panel shows the fit of a three-component model (see Table 4 for the parameters) to the summed spectrum from both the Sgr and Sct regions. The right panel is the unfolded spectrum displaying each of the three components and the assumed CXRB.

intensity ratio of ∼2:1 is the value expected from a plasma in collisional ionization equilibrium at $kT \sim 10$ keV. Therefore, *nei* is not the case unless the temperature is much higher than 10 keV.

If instead the hot plasmas are in ionization equilibrium, they must consist of multiple temperature components in order to account for the lines from lower-Z elements than Fe. For instance, the observed H-like to He-like line intensity ratios of Si and S correspond to $kT \sim 0.9$ keV and ∼1.5 keV, respectively. Therefore, the temperature distribution should span over these temperatures. An attempt is made to reproduce the observed spectrum with a multi-temperature plasma model. The added spectrum of those from the Sct and Sgr regions are used for fitting. As expected, at least three components are required for obtaining a reasonable reproduction of the H-like/H-like line intensity ratios of Si, S and Fe. An example of a three-temperature model fit (nearly acceptable: $\chi^2_{\rm r} = 1.5$) is shown in Fig. 4 with the best-fit parameters listed in Table 4. A similar result is also obtained for the spectrum of the GC region.

Table 4. The best-fit parameters of a three-temperature plasma model for the observed spectrum from the Sct and Sgr regions (added).

Component	Temperature keV	Abundance Solar	$N^*_{\rm H}$ 10^{22} cm^{-2}
1. low	0.75	0.14	1.2
2. medium	1.8	0.24	4.3
3. high	10 (fixed)	0.68	18 ($> 12^\dagger$)

† 90% confidence lower limit.

Although such a multi-temperature model yields a qualitative reproduction of the observed spectrum, the model implies a rather unrealistic situation. The higher the temperature of the plasma component the larger is the absorption, which is necessary in order to accommodate lower temperature components. As a consequence, the absorption column required for the 10-keV component far exceeds the total interstellar column. This inconsistency seems to be inevitable.

Since the presence of a non-thermal tail has been well established, correct interpretation of the GRXE should also include it. Valinia et al. (2000b) recently published a model including the non-thermal component. They accounted for the ASCA GIS and the RXTE/OSSE spectra of the Sct region with a model consisting of two-temperature thermal components (in ionization equilibrium) and non-thermal emission by low-energy cosmic-ray electrons interacting with the interstellar medium. With this model they obtained the best-fit temperatures of the two plasma components to be ∼0.6 keV and ∼2.8 keV, respectively. The temperature of the soft component is similar to that of Kaneda et al. The inclusion of the Bremsstrahlung by low-energy cosmic-ray electrons reduced the temperature of the hotter plasma to $kT \sim 3$ keV. In their model, the iron K-line is a mixture of the 6.4-keV line from K-ionization of interstellar Fe atoms and the thermal 6.7-keV He-like line. The 7-keV H-like line is negligibly weak for a plasma temperature of $kT \sim 3$ keV. This is, however, in contradiction with the observed SIS spectrum that clearly shows the significant H-like line and requires a much higher plasma temperature, i.e. $kT \geq 7$ keV. Thus, the composite model fails to explain the observed spectrum as long as the bulk of the GRXE below 10 keV is interpreted to be thermal.

Some contribution from low-temperature ($kT \leq 1$ keV) plasmas of SNR origin may well be present. However, the hot plasma hypothesis for the bulk of the harder GRXE is questionable also from a general consideration on the nearly identical spectral shape in all the observed regions. Suppose the hot plasmas in these regions were produced by a similar, though yet unknown, mechanism. The thermal history of the plasmas should be

quite different between the GC region and other two regions, since their later evolution is strongly influenced by the environment. The gas density and magnetic fields are more than an order of magnitude different among these regions (e.g. Mezger et al. 1996). For instance, the expansion will be faster in a region of lower gas density and lower magnetic fields, and vice versa. This will cause a significant difference in the plasma temperature by adiabatic cooling. Thus, such close spectral similarity is difficult to explain.

On top of what is discussed above, the most severe problem for the thermal origin of the emission lines is the observed line broadening. The He-like and H-like Fe K-lines in the GC region are found to be significantly broad, corresponding to a line-of-sight velocity dispersion of the Fe ions of $\sim$3300 km s^{-1} (Tanaka et al. 2000). The rms velocity would be $\sim$5000 km s^{-1} for random motions. For the other two regions, the 90% confidence limit of the line width clearly indicates that these lines are similarly broadened, although the poorer statistics do not allow precise determination of the line widths. Such a high velocity of ions cannot be of thermal motion. (The velocity corresponds to a plasma temperature of several MeV.) Bulk plasma motions such as expansion or turbulence are also unlikely, because the inferred velocity far exceeds the sound velocity in a plasma of $kT \sim 10$ keV ($\sim$1200 km s^{-1}). Thus, apart from the fundamental problems of hot plasma hypothesis mentioned in Sect. 1, the present results show that the observed spectrum itself reveals crucial inconsistency in the interpretation of the GRXE in terms of thermal emission.

As regards the non-thermal continuum that extends beyond 100 keV, Valinia et al. (2000b) conclude that low-energy cosmic-ray electrons are the most probable origin. These electrons also produce 6.4-keV line by K-ionization of interstellar Fe atoms. If the interstellar medium has cosmic abundances, the equivalent width is of the order of 100 eV of the Bremsstrahlung continuum (Valinia et al. 2000b). However, the observed 6.4-keV lines in the Sgr and Sct regions (see Table 3) are much weaker than their model predicts. The 6.4-keV line is intense only near the GC, and diminishes sharply within 1° from the GC. This is most probably the fluorescence line from X-ray illuminated dense molecular clouds that are exceptionally abundant in the GC region. The deficiency of the 6.4-keV line may be understood as due to lower interstellar Fe abundance. In fact, the optically measured Fe abundance of interstellar gas is low (e.g. Savage & Sembach 1996), indicating that the metallic elements reside preferentially in dust grains. If the low-energy electrons could not penetrate these dust grains, the 6.4-keV line intensity would be lower than when all Fe atoms are in gaseous form. Hence, the weakness of the 6.4-keV line may not be against the presence of the electron Bremsstrahlung component.

An alternative possibility for the origin of the emission lines has been proposed, which considers charge exchange interaction of low-energy cosmic-ray heavy ions with interstellar hydrogen (Tanaka et al. 1999). The charge exchange interaction of low-energy heavy ions is an efficient process of producing emission lines. If low-energy cosmic-ray electrons are responsible for the hard continuum and are accelerated by a mechanism that depends only on the charge (as the Fermi acceleration), the same mechanism must also accelerates protons and heavy nuclei. The thus-produced low-energy cosmic-ray heavy ions will slow down by ionization loss when they go into neutral interstellar gas. The charge exchange cross section depends strongly on the ion energy (see e.g. Phaneuf et al. 1987). For the interaction of Fe^{+q} ions with H or H_2, the cross section rises steeply as the ions lose energy, in proportion to $E^{-4.5}$ when $Eq^{-1/2} \gg 25$ keV/nucleon. Whereas, for $Eq^{-1/2} < 25$ keV/nucleon, it is essentially constant at a large value around $10^{-15} \times q$ cm^2. Therefore, most interactions will take place at energies around $25q^{1/2}$ keV/nucleon. This energy corresponds to a velocity of $Fe^{+25\sim26}$ ions of $\sim$5000 km s^{-1}, and hence provides natural explanation of the observed broadening of the Fe lines.

The same process may also explain the emission lines of lower Z ions. Tanaka et al. (1999) pointed out that the relative intensities of the observed lines of individual elements exhibit fair similarity to the cosmic abundances and/or cosmic-ray abundances, which gives support to the low-energy cosmic-ray origin of the observed emission lines. A decisive test is to measure the widths of the lines from lower-Z elements. If the lines are indeed due to charge exchange interactions, similar Doppler broadening to that observed in the Fe K-lines is expected. If this were proven to be the case, the GRXE should provide information on the low-energy cosmic-rays that is otherwise inaccessible by other means. The SIS resolution is insufficient to measure the widths of those lines other than the Fe K-lines. Higher-resolution measurements of the diffuse GRXE emission with the grating spectrometers on the current X-ray missions would be difficult, and may have to await a future mission for a definitive answer. It is also worth noting that other spiral galaxies may as well emit diffuse hard X-rays similar to the GRXE. Such observations are urged.

Acknowledgements. The author thanks Y. Ikebe, R. Fujimoto, E. Miyata for their helps and H. Inoue for useful discussions.

References

Ebisawa, K., Maeda, Y., Kaneda, H., et al. 2001, Science, 293, 1633
Dickey, J. M., & Lockman, F. J. 1990, ARA&A, 28, 215
Dame, T. M., Hartmann, D., & Thaddeus, P. 2001, ApJ, 547, 792
Gendreau, K. C., Mushotzky, R., Fabian, A. C., et al. 1995, PASJ, 47, L5
Kaneda, H. 1997, Ph.D. Thesis, Univ. of Tokyo, ISAS RN 642
Kaneda, H., Makishima, K., Yamauchi, S., et al. 1997, ApJ, 491, 638
Koyama, K., Maeda, Y., Sonobe, T., et al. 1996, PASJ, 48, 249

Makishima, K. 1997, in X-Ray Imaging and Spectroscopy of Cosmic Hot Plasmas, ed. F. Makino (Tokyo: Universal Academy Press), 137
Mezger, P. G., Duschl, W. J., & Zylka, R. 1996, A&AR, 7, 289
Murakami, T., Tanaka, Y., Kulkarni, S. R., et al. 1994, Nature, 368, 127
Phaneuf, R. A., Janev, R. K., & Hunter, H. T. 1987, in Nuclear Fusion (Vienna: International Atomic Energy Agency), 13
Savage, B. D., & Sembach, K. R. 1996, ARA&A, 34, 279
Tanaka, Y., Miyaji, T., & Hasinger, H. 1999, Astron. Nachr., 320, 181
Tanaka, Y., Koyama, K., Maeda, Y., et al. 2000, PASJ, 52, L25
Tanuma, S., Yokoyama, T., Kudoh, T., et al. 1999, PASJ, 51, 161
Valinia, A., Kinzer, R. L., & Marshall, F. E. 2000a, ApJ, 534, 277
Valinia, A., Tatischeff, V., Arnaud, K., et al. 2000b, ApJ, 543, 733
Yamasaki, N. Y., Takahara, F., & Yamauchi, S. 1994, in New Horizon of X-Ray Astronomy, ed. F. Makino, & T. Ohashi (Tokyo: Universal Academy Press), 535
Yamauchi, S., & Koyama, K. 1993, ApJ, 404, 620
Yamauchi, S., Kaneda, H., Koyama, K., et al. 1996, PASJ, 48 L15
Worrall, D. M., Marshall, F. E., Boldt, E. A., et al. 1982, ApJ, 255, 111